26 May 2010, 4:45 pm - 6:45 pm

Numerical Analysis of Disconnected Spread Footing on Soft Soil During Strong Earthquake

Sascha Richter
Bilfinger Berger Civil, Germany

Roberto O. Cudmani
Bilfinger Berger Civil, Germany

Fifth International Conference on
Recent Advances in Geotechnical Earthquake Engineering and Soil Dynamics
and Symposium in Honor of Professor I.M. Idriss
May 24-29, 2010 • San Diego, California

NUMERICAL ANALYSIS OF DISCONNECTED SPREAD FOOTING ON SOFT SOIL DURING STRONG EARTHQUAKE

Sascha Richter
Bilfinger Berger Civil
65189 Wiesbaden, GERMANY

Roberto O. Cudmani
Bilfinger Berger Civil
65189 Wiesbaden, GERMANY

ABSTRACT

For the design of the Golden Ears approach bridge in Vancouver (Canada) a disconnected spread footing (DSF) was considered as alternative to a conventional pile foundation. In a DSF, a spread footing rests on natural ground improved by piles. Footing and piles are separated by a layer of coarse grained material. The mechanisms governing the behavior of the DSF during strong earthquake events have been investigated in a numerical finite element (FE) analysis using a (visco-)hypoplastic constitutive relationship. The FE model consists of a soil column (height 45 m) which includes the concrete piles. The superstructure is represented by a point mass attached to the end of a vertical beam. Material parameters for the constitutive law were derived from available field and laboratory tests. The numerical model was validated using results of large-scale in-situ tests, where a single-pile DSF was subjected to alternating vertical and horizontal loading. The goal of the numerical study was the investigation of the influence of pile spacing and gravel layer thickness on the dynamic foundation response and internal pile forces during a strong earthquake. Comparative calculations were carried out for a conventional pile foundation. A significant kinematic decoupling between footing and improved soft soil through the gravel layer did not occur in the simulations. Analysis results show that the internal forces in the piles of a DSF are significantly smaller compared with those in a conventional pile foundation, particularly in the upper part of the pile. However, in the investigated range, a dependence of bending moments and shear forces in the piles on the thickness of the gravel layer was not observed. On the other hand, the pile spacing in a DSF has a more pronounced influence on the internal pile forces.

INTRODUCTION

Floodplains of the Fraser River and its tributaries cover a large part of the Vancouver area (Canada). The subsoil conditions in the area of the river delta are characterized by young, water-saturated sediments of high compressibility, e.g. silt, clay and peat. Due to the poor mechanical properties of the natural soil, deep foundations and soil improvement are required in most cases to fulfill design requirements. The real challenge for the foundation design results from the combination of the poor natural ground with the high seismic hazard of the region, particularly the occurrence of strong earthquakes. In a conventional pile foundation piles are fixedly connected to a pile cap. Earthquake shaking leads to significant bending moments and shear forces in the piles, particularly in the upper soft soil layer, where the horizontal subgrade reaction is poor. In order to limit the internal forces of the piles, the number/diameter of piles is usually increased, which causes an increase of foundation stiffness. The stiffer foundation may induce even higher internal forces and lead to a further increase of the moment and shear force loading of the piles during the earthquake. In order to break this vicious circle, the disconnected spread footing (DSF) has been proposed. Principle, design and application of a DSF were described in several references, e.g. Pecker (2004).

The goal of this paper is to present results of a numerical investigation of a DSF which was envisaged for the foundation of the approaches to the Golden Ears Bridge over the Fraser River in Vancouver. In the analysis subsoil and foundation are subjected to horizontal shaking due to a strong earthquake event. In the next sections, the numerical model, the determination of soil parameters and the generation of the input ground motion are described. Main results of the study along with their interpretation and the analysis of the mechanisms governing the dynamic response of the DSF during strong earthquakes are presented.

PRINCIPLE OF DISCONNECTED SPREAD FOOTING

As opposed to a classical pile foundation where piles are structurally connected to a pile cap, a disconnected spread footing rests on top of natural ground reinforced with piles. Footing and piles are separated by a layer of coarse grained material, e.g. gravel. The principle configuration of a DSF is shown in Fig. 1. The piles, sometimes called inclusions (Pecker, 2004), ensure the transfer of vertical loads to deeper, more competent soil strata. The soil-pile composite exhibits better mechanical properties, i.e. higher strength and stiffness than the natural soft soil, and contributes to the fulfillment of limit and serviceability state requirements of the foundation for temporary and permanent vertical loads.

The disconnection between footing and piles is attained by a layer of coarse grained material. During a strong seismic event alternating shearing of the granular material causes a degradation of its shear stiffness and energy dissipation (hysteretic damping). If the magnitude of shear strain is large enough (the shear stiffness may decrease to 10% of its initial value for shear strain amplitudes of 1%) the transmission of shear waves through the gravel layer and consequently, the shear forces transferred from the ground to the superstructure may decrease significantly. In this case, a decoupling of the ground motion from the motion of the foundation and superstructure is expected to occur, i.e. the gravel layer acts more as an isolator than as a "plastic hinge" as indicated by Pecker (2004). As an additional mechanism, a decoupling of subsoil and superstructure can occur due to sliding of the footing on the gravel. This mechanism will be relevant once the horizontal forces exceed the maximum friction force at the interface footing-gravel. During sliding the interface between the gravel layer and the footing behaves as a "plastic hinge" in the sense of Pecker (2004).

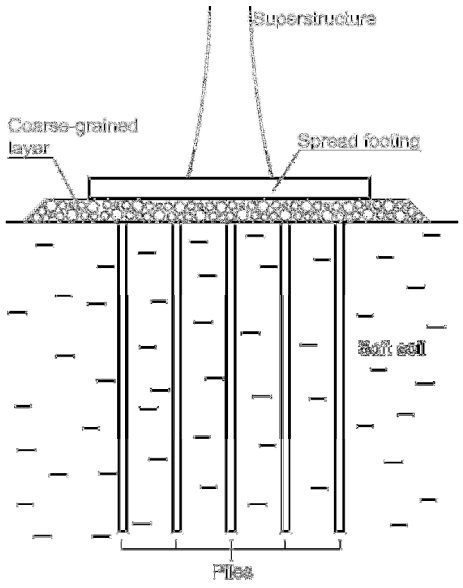

Fig. 1. Principle layout of disconnected spread footing on coarse-grained layer over soft soil.

GOAL OF THE NUMERICAL STUDY

The numerical investigation focuses on the influence of the pile spacing and the thickness of the gravel layer on:

- dynamic response of the superstructure,
- bending moments and shear forces in the piles,
- shear behavior of the coarse grained layer (gravel).

In order to evaluate these influences both the pile spacing *s* and the gravel layer thickness *d* were varied within realistic ranges. In addition to a DSF, a fixed connection between pile and footing (conventional pile foundation) was analyzed. The combinations investigated are shown in Table 1. Other influences, e.g. soil properties or seismic excitation, were not varied within the scope of the present work.

Table 1. Investigated combinations of pile spacing s and gravel layer thickness d.

		Pile spacing *s*			
		1.5 m	2.0 m	2.5 m	no pile
Thickness gravel layer *d*	0.25 m	-	yes	-	-
	0.50 m	yes	yes	yes	yes
	1.00 m	-	yes	-	-
Pile fixed to footing		-	yes	-	-

CONSTITUTIVE MODEL

A realistic simulation of the soft-soil behavior is essential for the reliable prediction of the behavior of the DSF during an earthquake. In order to accomplish this task, a visco-hypoplastic constitutive model was used for modeling the behavior of cohesive soils in the finite element (FE) analysis. The model takes into account the non-linear stress-strain behavior as well as the time- and rate-dependent soil behavior under monotonic and alternating shearing. The quasi-elastic behavior of granular material at very small strain is simulated with the help of an additional tensorial state variable (intergranular strain). A detailed description of the constitutive law can be found for example in Niemunis (2003).

The behavior of the non-cohesive material, i.e. the gravel base, was modelled using a hypoplastic constitutive relationship, whose details are discussed elsewhere, e.g. Niemunis and Herle (1997). The applicability of both constitutive laws to the solution of geotechnical problems have already been validated in the past, e.g. Bühler (2006), Karcher (2003), Libreros (2006). In particular, the applicability of hypoplasticity to the solution of geotechnical earthquake engineering problems, especially to the analysis of soil response during earthquake, was shown in Cudmani et al. (2003) and Gudehus et al. (2004).

A detailed description of the soil parameters used in the (visco-)hypoplastic formulation is outside the scope of this article but can be found elsewhere, e.g. Herle and Gudehus

(1999), Niemunis (2003). For the sake of completeness, a short explanation of the parameters for both constitutive laws is given below. Parameters for the hypoplastic law are as follows:

φ_c = friction angle at critical state,
h_s = granular hardness (parameter controlling the compressibility of the granular skeleton),
n = exponent which describes stress dependence of stiffness,
e_{d0}, e_{c0}, e_{i0} = limit void ratios for $p' \rightarrow 0$ in densest, critical and loosest state of the granular skeleton,
α and β = coefficients controlling influence of density on peak friction angle (pyknotropy coefficient) and stress rate (barotropy coefficient).

The following alternative parameters are required for the visco-hypoplastic formulation:

φ_c = friction angle at critical state,
λ = compression coefficient (Butterfield compression law),
κ = swelling coefficient (Butterfield compression law),
e_{100} = void ratio at reference pressure p' = 100 kPa, OCR=1 and $\dot{\varepsilon} = \dot{\varepsilon}_r$,
$\dot{\varepsilon}_r$ = reference strain rate = creep rate for OCR=1,
β = controls shape of yield surface,
I_v = viscosity index ($\approx C_\alpha/C_c$).

For the description of the quasi-elastic small-strain behavior the following parameters are required:

m_T, m_R = control small-strain stiffness after 90° and 180° reversal of strain rate direction,
R_{max} = controls the size of the quasi-elastic strain range,
β_χ = controls evolution of intergranular strain,
χ = controls degradation of small-strain stiffness during monotonic deformation.

GROUND CONDITIONS

In general, the geology of the Vancouver area is characterized by sandstone bedrock, which can reach a thickness of several kilometers. The sandstone is overlain by ice age sediments (e.g. till) with a thickness of up to 1 km. Modern sediments, which are less than 10,000 years old (i.e. Holocene age), have been deposited by the Fraser River in low-lying areas. These deposits consist of water-saturated sand, silt, clay and peat in a loose/soft state. They can reach depths of more than 100 m.

The subsoil at the location of the planned DSF can roughly be divided into two zones. The upper Zone 1 consists of clayey silt, organic silt and peat. These soils are in a soft to firm state. The thickness of Zone 1 is about 10 m to 25 m. Zone 2 consists of firm to stiff silty clay. It is more than 100 m thick. A further subdivision of Zone 1 (1A, 1B) and Zone 2 (2A, 2B) for the present analysis was done based on in-situ and lab test results, which are discussed below.

DETERMINATION OF SOIL PARAMETERS

In the present study constitutive parameters and the initial state of the soil were estimated based on available field and laboratory test results. The initially estimated constitutive parameters were validated by back calculations of a large-scale in-situ test with a DSF.

For the estimation of constitutive parameters, results from oedometric tests, cyclic simple shear tests and triaxial tests were considered. Oedometric test results were used for the estimation of compressibility parameters of the visco-hypoplastic constitutive law. The experimental compression curves were fitted using numerical element test simulations (direct integration of the constitutive equations). Initial state and test conditions were adopted, while the governing visco-hypoplastic parameters, i.e. λ, κ and e_{100}, were adapted until a satisfactory fit of the loading and unloading paths was achieved. Experimental results are exemplarily presented along with numerical results for the soft soil of Zone 1 and Zone 2 in Fig. 2. As shown, the constitutive model is able to describe the compressional behavior of the soils during loading, unloading and reloading realistically.

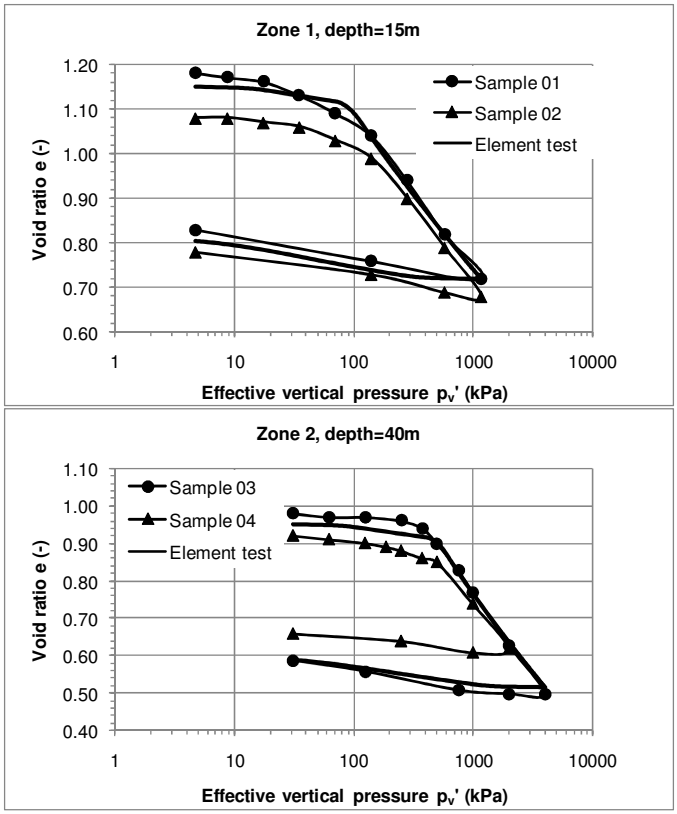

Fig. 2. Results of laboratory compression tests and numerical element tests for soil in Zone 1 (top) and Zone 2 (bottom).

Furthermore, numerical cyclic simple shear tests (strain controlled) were performed using the visco-hypoplastic constitutive law for the determination of the intergranular strain parameters R_{max}, m_T, m_R, β_χ and χ. For each shear strain amplitude γ a number of five shear cycles was simulated. The last shear cycle was analyzed in order to determine the shear

modulus G and the equivalent viscous damping ratio D of the sample for the specific value of γ. The numerical results are compared to results from laboratory cyclic simple shear tests (CSS) which were executed at relatively high strain amplitudes. Furthermore, empirical relationships of G/G_{max} and D versus γ for cohesive soils (PI=30) proposed by Vucetic and Dobry (1991) were adopted. In order to obtain G from the empirical results, the values of G/G_{max} was multiplied with the value of $G_{max}=G(\gamma=1\cdot10^{-6})$ from the numerical test. As can be seen in Fig. 3, the decay of G and the increase of D with γ as derived from Vucetic and Dobry (1991) agree reasonably with the predicted developments of G and D. The calculated damping ratio D exceeds the empirical values by about 50% at strain amplitudes $\gamma>10^{-3}$. Nevertheless, the deviation is not significant as long as the shear strain does not significantly exceed $\gamma=10^{-3}$. The laboratory test results show a reasonably good agreement with the numerical predictions for the shear strain range investigated.

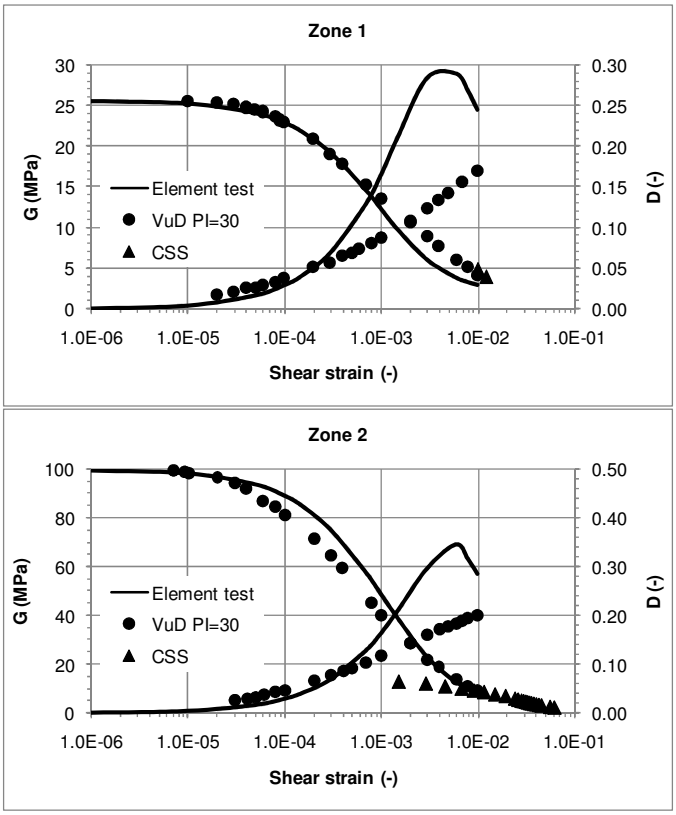

Fig. 3. Evolution of G and D vs. shear strain amplitude from numerical element tests, laboratory cyclic simple shear tests (CSS) and empirical relationship of Vucetic and Dobry (1991) (VuD) for representative soil elements in Zone 1 (top) and Zone 2 (bottom).

The mechanical behavior of the gravel layer between the bottom of the footing and the top of the piles was modeled via a hypoplastic constitutive equation. Information concerning the properties of the gravel used in the field tests was unavailable. Therefore, typical parameters for gravel were adopted from Schünemann (2006).

The final sets of parameters used for the analysis are presented in Table 2 and Table 3 for the visco-hypoplastic and hypoplastic constitutive relationship, respectively.

Table 2. Parameters of the visco-hypoplastic constitutive relationship for the soft soil layers.

Parameter		Layer			
		1A	1B	2A	2B
φ_c	[°]	27	27	30	30
λ	[-]	0.060	0.100	0.120	0.110
κ	[-]	0.012	0.014	0.013	0.013
e_{100}	[-]	1.00	1.25	1.40	1.20
β	[-]	0.6	0.6	0.6	0.6
I_v	[-]	0.030	0.030	0.035	0.035
$\dot{\varepsilon}_r$	[1/s]	$1\cdot10^{-6}$	$1\cdot10^{-6}$	$1\cdot10^{-6}$	$1\cdot10^{-6}$
m_T	[-]	7.0	7.0	7.0	7.0
m_R	[-]	7.0	7.0	7.0	7.0
R_{max}	[-]	$1\cdot10^{-4}$	$1\cdot10^{-4}$	$1\cdot10^{-4}$	$1\cdot10^{-4}$
β_χ	[-]	0.1	0.1	0.1	0.1
χ	[-]	1.0	1.0	1.0	1.0

Table 3. Parameters of the hypoplastic constitutive relationship for the gravel layer.

Parameter		Gravel
φ_c	[°]	50
hs	[MPa]	150
n	[-]	0.40
e_{d0}	[-]	0.65
e_{c0}	[-]	1.00
e_{i0}	[-]	1.15
α	[-]	0.05
β	[-]	4.0
m_T	[-]	5.0
m_R	[-]	5.0
R_{max}	[-]	$1\cdot10^{-4}$
β_χ	[-]	0.2
χ	[-]	1.0

DETERMINAITION OF INITIAL SOIL STATE

The evaluation of the initial state of the cohesive soil layers (in-situ density, state of stress, OCR) was based on both the results of CPT as well as physical and index tests on undisturbed soil samples. In the framework of the visco-hypoplastic constitutive model a relationship exists between the void ratio e, the overconsolidation ratio (OCR) and the stress state, i.e. if two variables are defined, the third one can be unambiguously determined.

In our study, the effective stress state was calculated from the unit weights and a horizontal earth pressure coefficient of $K_0 = 0.6$. The initial OCR was estimated from CPT results based on empirical relationships proposed by Mayne (1991) and Lunne et al. (1997). With this object, several CPTs in

close proximity to the site of the DSF were analyzed. Figure 4 shows typical cone resistances and pore pressures with depth. The distribution of OCR derived from CPT results and the approximation used in the numerical modeling are shown in Fig. 5. Based on the effective stress state and the OCR distribution, the initial void ratio distribution was determined from the constitutive model. For validation purposes, the calculated void ratios were compared with the values obtained from undisturbed soil samples at different depths.

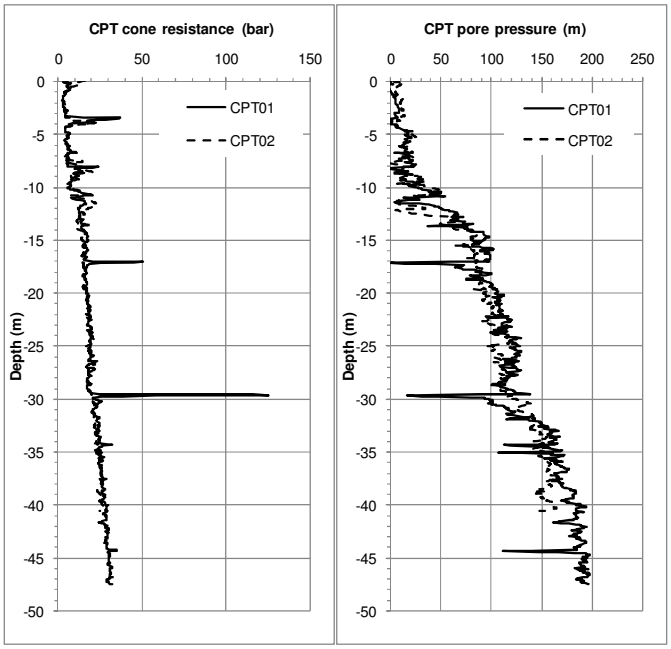

Fig. 4. Results of two typical CPTs. Left: cone resistance vs. depth, right: pore pressure vs. depth.

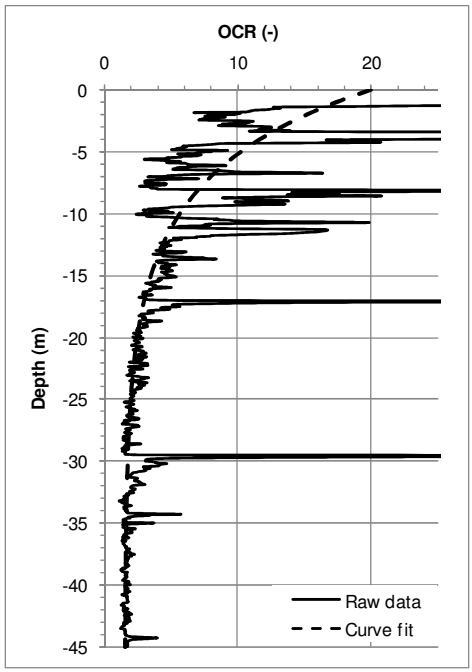

Fig. 5. Overconsolidation ratio OCR vs. depth derived from nearby CPT results (solid line) and curve fit (dashed line).

NUMERICAL MODEL

For the numerical analysis of the DSF the finite element (FE) software ABAQUS (version 6.8) was employed. In order to realistically simulate the interaction of footing, soil and pile two 3D-models were developed assuming that the piles are installed in a regular rectangular grid with a constant pile spacing (see Fig. 6):

(i) model for a center pile of the DSF foundation,
(ii) model for an edge pile.

The first model applies to a pile which is surrounded by other piles and which is far away from the edge of the footing. Due to symmetry only half a pile is modeled along with the corresponding soil mass. The FE model is presented in Fig. 7. The model consists of approx. 4,500 elements and 6,500 nodes.

The dynamic response of edge piles is influenced by the pile group on one side and by the existing natural soil on the other side. Therefore, a section crossing the entire DSF needs to be considered for a realistic analysis of an edge pile (Fig. 6). In order to limit the model size, the outer piles were modeled with continuum elements while the inner piles are modeled with beam elements. The model is shown in Fig. 8. The model consists of approx. 11,500 elements and 16,000 nodes.

Similar boundary conditions have been applied to both models. Periodic displacement boundary conditions can be applied at the faces that point into the x-direction (direction of input ground motion) and u_y=0 at the faces that point into the y-direction (u=nodal displacement). The bottom of the model is fixed in all direction (u_x=u_y=u_z=0) during static calculation steps. During the earthquake (dynamic step) the corresponding displacement is prescribed at the bottom of the model in x-direction, i.e. $u_x \neq 0$.

The contacts between spread footing and gravel, gravel and pile, and pile and soil have been simulated via Coulomb friction. Sliding and separation of the footing on top of the gravel was enabled. Non-sliding contacts have been considered acceptable for the simulation of the pile-soil contact as relative displacements are expected to be negligible. The contact properties are listed in Table 4.

Table 4. Contact properties and parameters used in FE analysis.

Contact	Contact behavior	
	Normal	Tangential
Footing – gravel	Hard contact, separation possible	μ=0.57
Gravel – pile	Hard contact, separation not poss.	μ=0.57
Pile – soil	Hard contact, separation not poss.	μ=∞ (no slip)

For the representation of the influence of the superstructure on the behavior of the foundation during seismic loading, the distributed mass of the superstructure has been reduced to a point mass. This point mass rests on top of a beam representing the bridge pier which connects footing and superstructure. Point mass and beam stiffness have been scaled according to the size of the investigated model. Only the results of the center-pile model will be presented in this article.

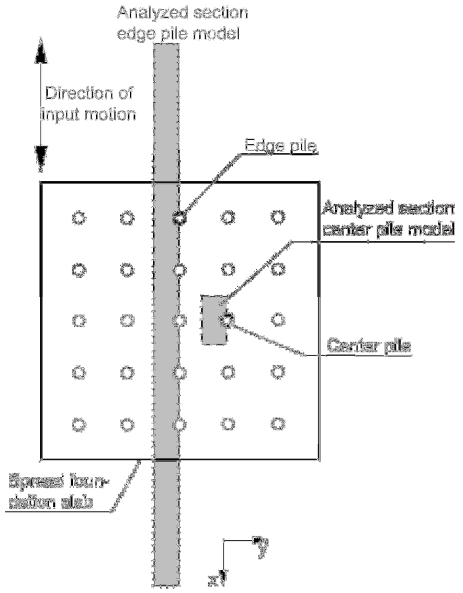

Fig. 6. Top view of disconnected spread footing with regular rectangular pile pattern, location of center pile and edge pile and corresponding model section (grey).

VALIDATION OF NUMERICAL MODEL AND SOIL PARAMETERS

Large-scale field load tests were performed with two spread footings each resting on a gravel layer (d=0.2 m) over a single pile with a diameter of 0.35 m. During these tests the footings were cyclically loaded in both vertical and horizontal direction and the induced displacements of the footings were recorded. In order to validate our model, the tests were back-calculated numerically. For the sake of simplicity, only a few load cycles were analyzed numerically. In general, the results, which are not shown here, validated the set of constitutive parameters presented in Table 2 and Table 3 and the contact parameters in Table 4.

EARTHQUAKE INPUT GROUND MOTION

The Landers earthquake 1992 (record station Joshua Tree) was adopted for the investigation of the behavior of the DSF. The corresponding acceleration record is spectrally matched to a target firm-ground motion at an outcrop location representtative of the Vancouver area for a return period of 2475 years. Acceleration- and displacement-time histories are shown in Fig. 9. The displacement obtained from the integration of the uncorrected acceleration signal drifts significantly with time.

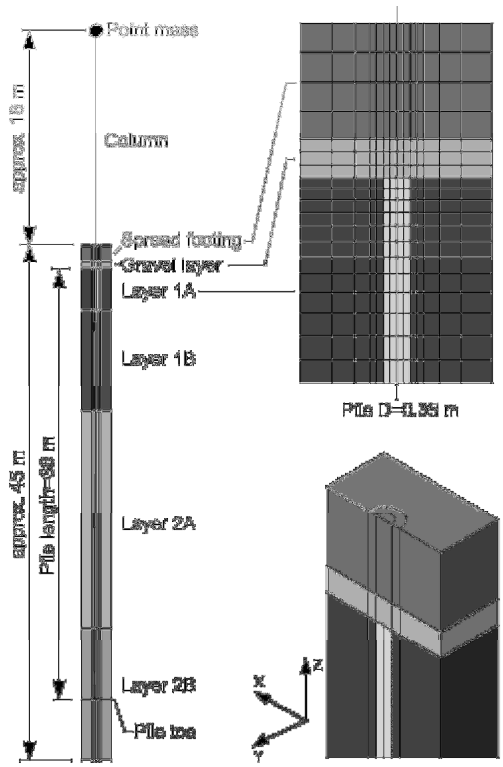

Fig. 7. Model of center pile. Left: complete model with soil layers, column and point mass. Top right: detail of upper part with FE mesh. Bottom right: 3D view of upper part of model.

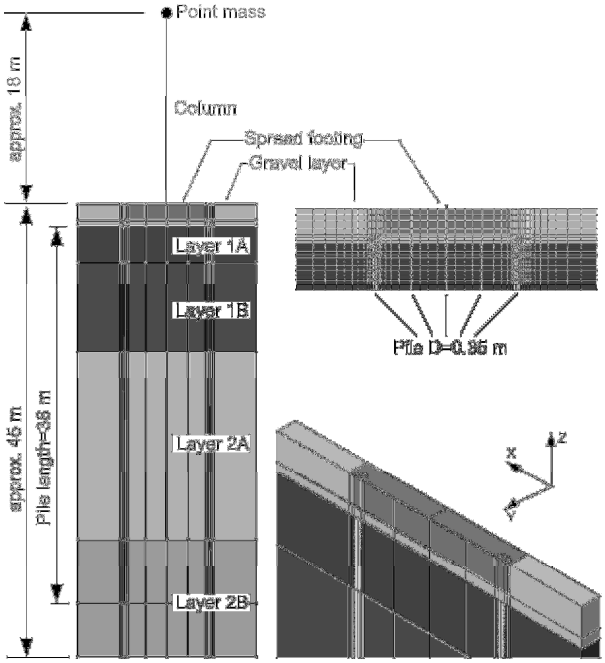

Fig. 8. Model of edge pile. Left: complete model with soil layers, column and point mass. Top right: detail of upper part with FE mesh. Bottom right: 3D view of upper part of model.

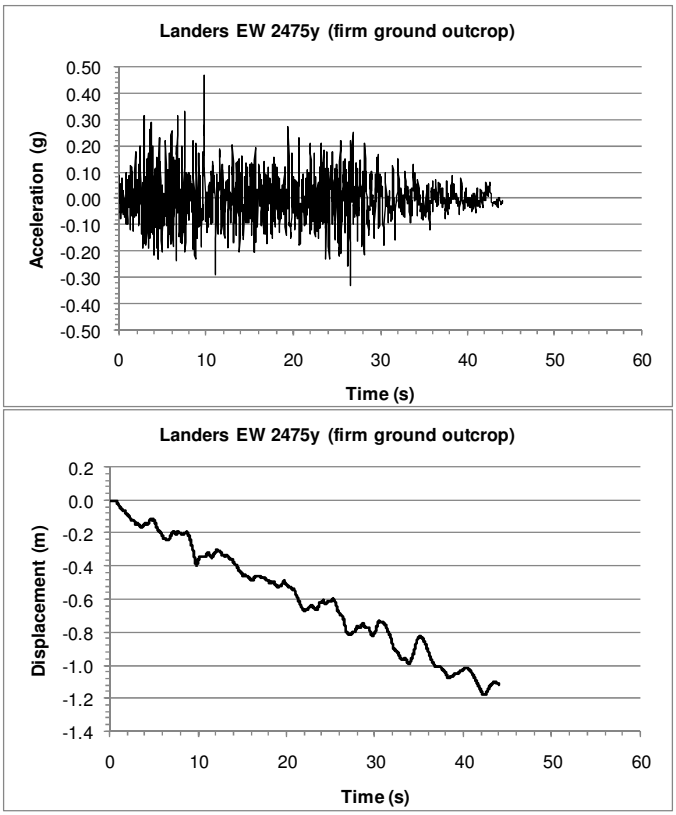

Fig. 9. Acceleration- and displacement-time histories for spectrally matched earthquake signal at rock outcrop (Landers 1992, Joshua Tree).

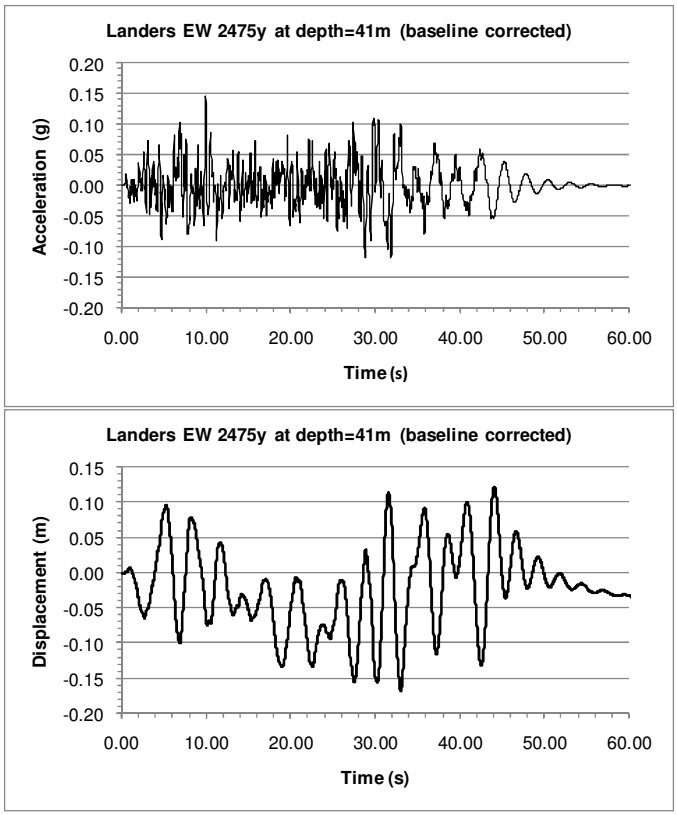

Fig. 10. Acceleration- and displacement-time histories for earthquake signal at depth=41 m derived from spectrally matched rock outcrop signal (Fig. 9).

In order to generate the input ground motion at the bottom of the numerical model (depth=41 m) the following procedure was followed:

1. Baseline correction of firm ground outcrop record shown in Fig. 9.
2. 1D equivalent linear ground response analysis (Shake2000) to produce acceleration at a depth of 150 m (assumed depth of bedrock) for firm ground conditions (input motion=output motion from step 1).
3. Baseline correction of ground motion at depth=150 m (output motion from step 2) using the correction method provided in Shake2000 (parabolic method).
4. 1D equivalent linear ground response analysis (Shake2000) with model representing in-situ soil conditions to produce displacement signal at a depth of 41 m (input motion=output motion from step 3). In-situ shear wave velocities for shake analysis were derived from results of seismic cone penetration tests (SCPT). Typical results are exemplarily shown in Fig. 11.
5. Baseline correction of acceleration at depth=41 m (output motion from step 4).

The resulting acceleration- and displacement-time histories are shown in Fig. 10. The displacement-time history was used as base excitation in the FE analysis.

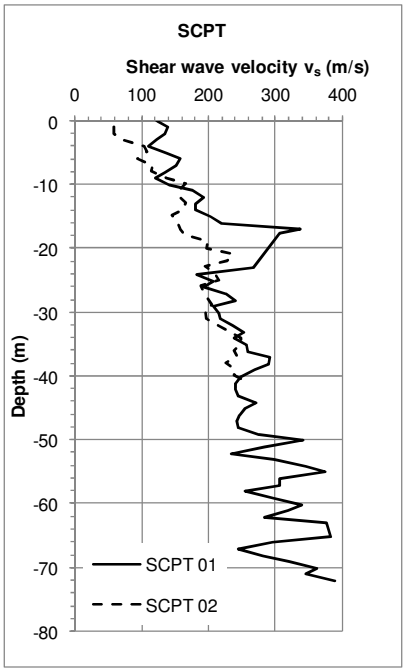

Fig. 11. Measured shear wave velocities from seismic cone penetration tests (SCPT).

NUMERICAL SIMULATION

The following stages were considered in the numerical analysis:

1. Generation of in-situ stress state,
2. Pile installation,
3. Construction of gravel layer and spread footing,
4. Construction of the pier and the superstructure on top of spread footing,
5. Simulation of the earthquake.

In order to achieve numerical convergence during step 5, maximum time increments were kept at Δt=0.002 s. This time increment results in 30,000 analysis steps for an earthquake duration of 60 s. The resulting total time for the analysis of one center pile model was in the range of 7 days with a workstation (Dell, CPU Intel Xeon 5160, 3 GHz, user memory=16 GB, OS Linux/x86-64).

RESULTS AND INTERPRETATION

For the evaluation of the influence of the gravel layer thickness d and the pile spacing s on the dynamic response of the DSF, the time-displacement behavior of the numerical model, the bending moments and shear forces in the piles as well as the shear behavior of the gravel layer and soft soil were evaluated.

Time-displacement behavior

The horizontal displacement of the superstructure (represented by the point mass) and the footing are considered important criteria for the evaluation of the foundation performance. The kinematic behavior of the point mass for different pile spacings s and gravel layer thicknesses d is shown in Fig. 12 and Fig. 13, respectively. Maximum displacements are in the range of 0.4 m to 0.5 m and occur during the period of strong shaking. The displacement amplitude of the point mass does not show any significant dependence on pile spacing. Even without piles the displacement amplitude is very similar to that obtained with ground reinforcement. Fig. 13 shows that the influence of the thickness of the gravel layer on the kinematic response of the superstructure is also insignificant in the investigated range. The maximum value of horizontal displacement is observed for d=1.0 m. Similar conclusions can be drawn from the acceleration-time histories of the superstructure (not shown).

The displacement amplitudes of the footing are smaller than those of the point mass. Maximum values are in the range of 0.3 m to 0.4 m as shown in Fig. 14 and Fig. 15. With exception of the conventional pile foundation (piles connected to the footing), a permanent displacement of the footing of about 10 cm is induced by the earthquake. The permanent displacement results mainly from plastic shear deformations in the soil column. There is a tendency for slightly higher displacement values for the DSF with the smallest pile spacing (s=1.5 m) and the thickest gravel layer (d=1.0 m). In the case of no pile (only soft soil and gravel layer with d=0.5 m) the displacements of the footing are comparatively small, i.e. the presence of the pile allows a better transition of shear forces to the footing. In all cases investigated the displacement-time histories of the footing are very similar to those in the upper part of the natural soil (not shown).

Resuming, neither a significant influence of pile spacing and gravel layer thickness on the kinematic behavior nor a decoupling of the foundation motion from the ground motion could be observed in the calculations.

Bending moments and shear forces in the piles

Bending moments and shear forces along the pile were evaluated during the earthquake. Envelopes of the maximum absolute moments and forces have been determined. The calculated distribution of bending moments and shear forces are shown in Fig. 16 through Fig. 19. As can be seen, maximum moments and shear forces are developed in the upper part of the pile, i.e. at a depth of 0 m to about 15 m. The lower part of the pile (depth>20 m) is fixed in the soil and is hardly influenced by the earthquake impact.

As expected, bending moments increase with decreasing pile spacing (see Fig. 16). This effect is stronger in the upper part of the piles where the stiffness of the soft soil is the smallest and therefore, the effect of reinforcing elements is the strongest. A similar dependency on pile spacing can be observed for the shear forces, as shown in Fig. 18. On the contrary, a significant influence of the gravel layer thickness on pile bending moments and shear forces was not found (see Fig. 17 and Fig. 19).

For the DSF, the ultimate moment capacity of 134 kNm of the considered reinforced concrete pile is well above the maximum calculated values of about 35 kNm. Similarly, the ultimate shear force capacity of 50 kN was not exceeded in the numerical analysis, where maximum values of about 20 kN were determined. In contrast, a fixed connection between pile and footing leads to a drastic increase of bending moments and shear forces near the top of the pile. Maximum moments and shear forces are M_{max}=130 kNm and Q_{max}=660 kN, respectively. While the maximum bending moments in the numerical analysis are just below the ultimate moment capacity, shear forces exceed the ultimate shear force capacity by a factor of more than 10. This indicates that without disconnection of piles and footing a shear failure of the piles is expected to occur during the earthquake.

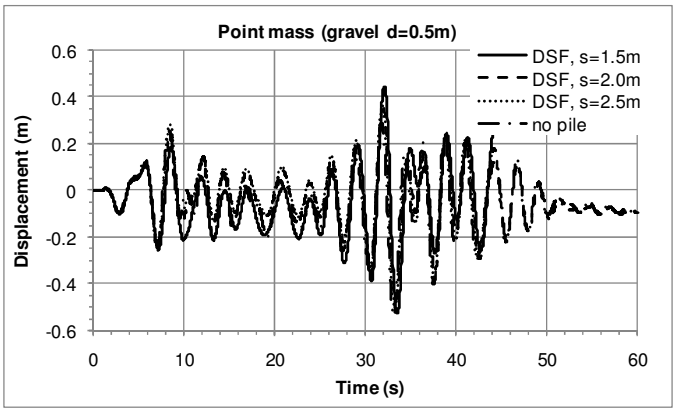

Fig. 12. Horizontal displacement of point mass with time: influence of pile spacing (gravel layer d=0.5 m; calculation for s=1.5 m not finished).

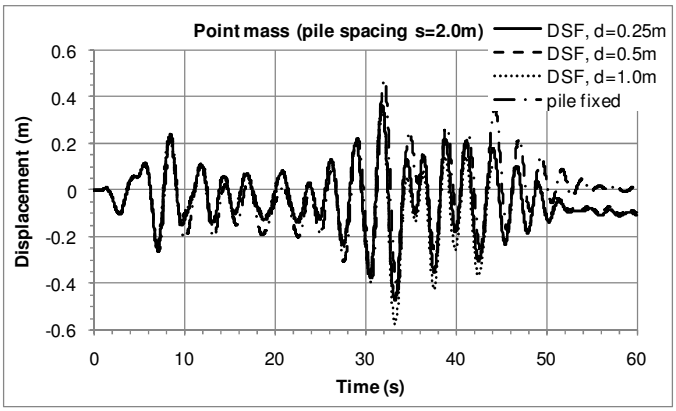

Fig. 13. Horizontal displacement of point mass with time: influence of thickness of gravel layer (pile spacing s=2.0 m).

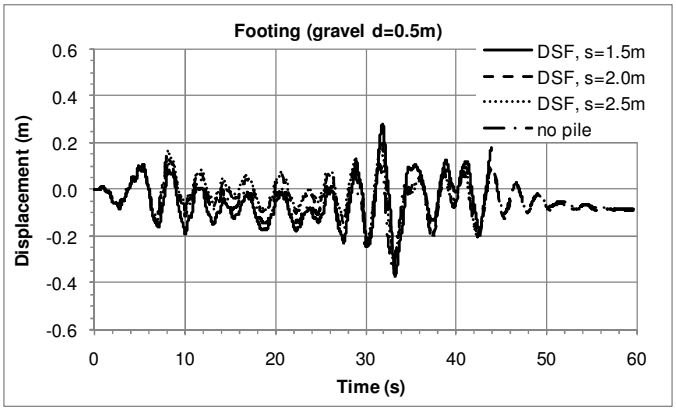

Fig. 14. Horizontal displacement of concrete footing with time: influence of pile spacing (gravel layer d=0.5 m).

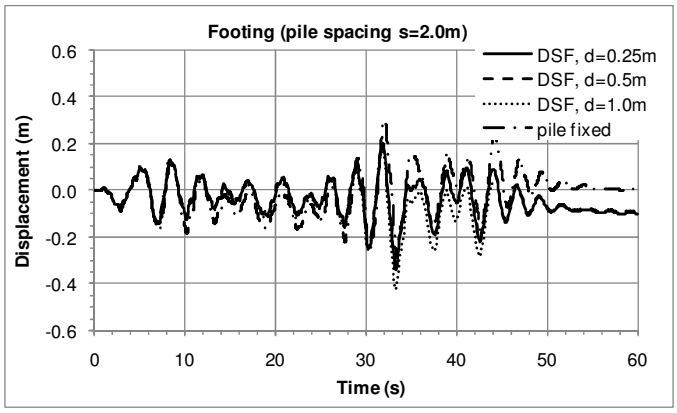

Fig. 15 Horizontal displacement of concrete footing with time: influence of thickness of gravel layer (pile spacing s=2.0 m).

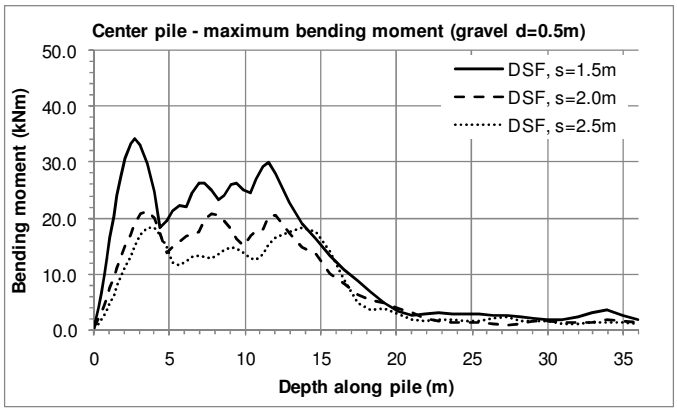

Fig. 16. Maximum bending moment along pile: influence of pile spacing (gravel layer d=0.5 m).

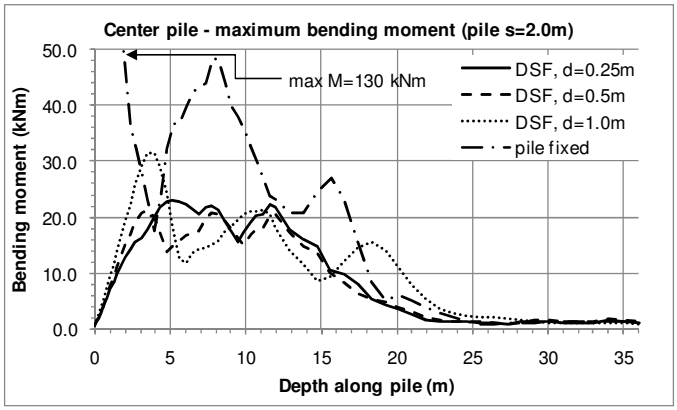

Fig. 17. Maximum bending moment along pile: influence of thickness of gravel layer (pile spacing s=2.0 m).

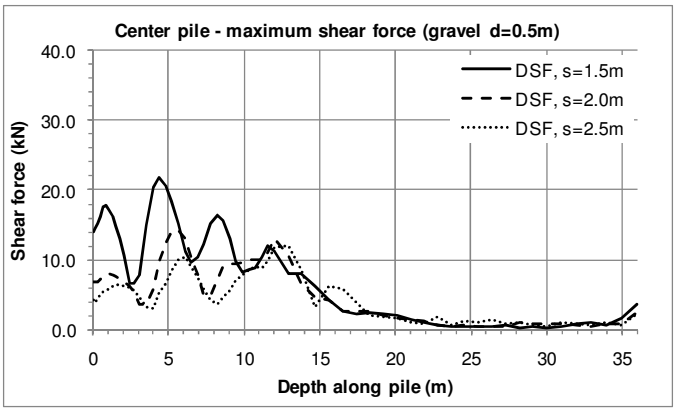

Fig. 18. Maximum shear force along pile: influence of pile spacing (gravel layer d=0.5 m).

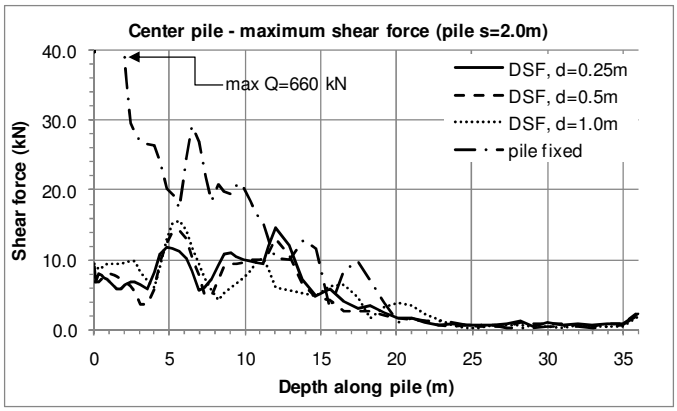

Fig. 19. Maximum shear force along pile: influence of thickness of gravel layer (pile spacing s=2.0 m).

Shear behavior of gravel layer

According to Pecker (2004), the gravel layer separating spread footing and piles is equivalent to a "plastic hinge" that yields in case of excessive horizontal shearing. In principle, two shearing mechanisms govern the coupling between ground and footing: shearing within the gravel layer and sliding at the interface between gravel layer and footing.

Relative displacements at the interface footing-gravel can be observed in the numerical model. Fig. 20 shows the differential horizontal displacement between spread footing and top of the gravel layer. For the DSF (d=0.5 m, s=2.0 m) maximum differential displacements of 7 mm are calculated, which are very small compared to the total displacement amplitudes of about 0.3 m at this location (Fig. 14, Fig. 15). Other DSF configurations show a very similar behavior. Fig. 21 shows the behavior of tangential contact stress to tangential displacement in the contact during the earthquake. The displacements at the contact are not large enough to mobilize the maximum sliding resistance, i.e. the contact behavior is elastic. A permanent displacement at the interface footing - gravel cannot be observed in the numerical analysis.

Energy dissipation within the gravel layer occurs due to the hysteretic behavior of the granular material. Fig. 22 and Fig. 23 show the hysteresis loops (shear stress vs. shear strain) in the gravel layer during the earthquake for the DSF (d=0.5 m, s=2.0 m) and the case of the pile fixed to the footing (s=2.0 m), respectively. In the case of the DSF, the shear strain reaches amplitudes γ of about $2 \cdot 10^{-3}$ with maximum shear stresses of approximately 40 kPa. The areas of the largest loops indicate an equivalent viscous damping ratio of D=15%. In the case of the pile fixed to the footing the shear stress developed in the gravel layer is small compared to the case of the DSF as vertical loads from footing and superstructure are transferred by the piles into deeper layers. Due to the small shear stresses a pronounced hysteretic behavior cannot be observed, see Fig. 23.

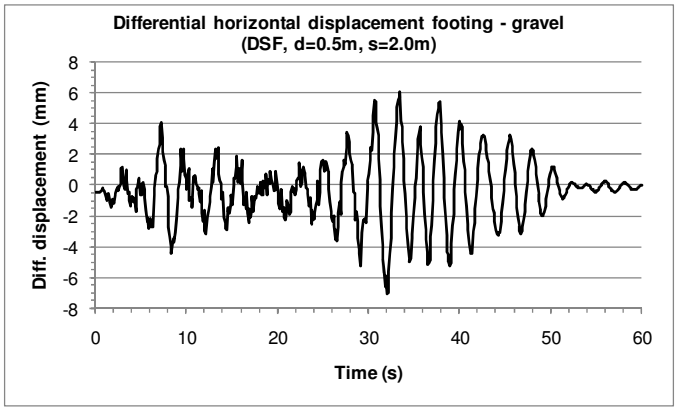

Fig. 20. Differential horizontal displacement between spread footing and top of gravel layer for DSF (d=0.5 m, s=2.0 m).

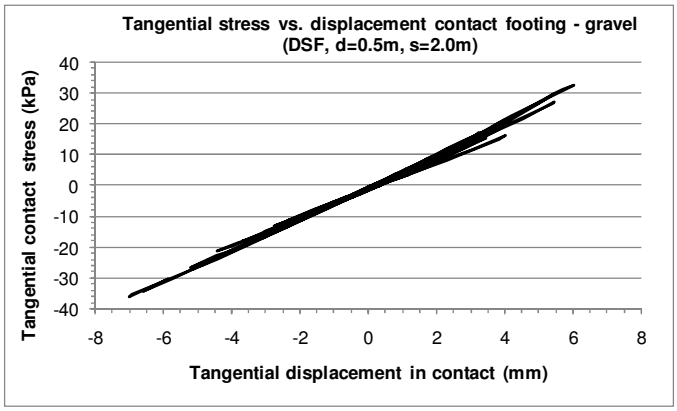

Fig. 21. Tangential contact stress vs. tangential contact displacement at contact footing - gravel for DSF (d=0.5 m, s=2.0 m) during earthquake (duration=60 s).

For comparison purposes Fig. 24 presents the hysteretic behavior of the soft soil underneath the gravel layer (depth approx. 1 m) for the case of the DSF (d=0.5 m, s=2.0 m). While shear stresses reach values similar to those in the gravel layer (Fig. 22), the shear strain amplitudes exceed those in the gravel by one order of magnitude due to the comparatively low stiffness of the improved soil. Hence, the energy dissipated in the soft soil is higher than that dissipated in the gravel.

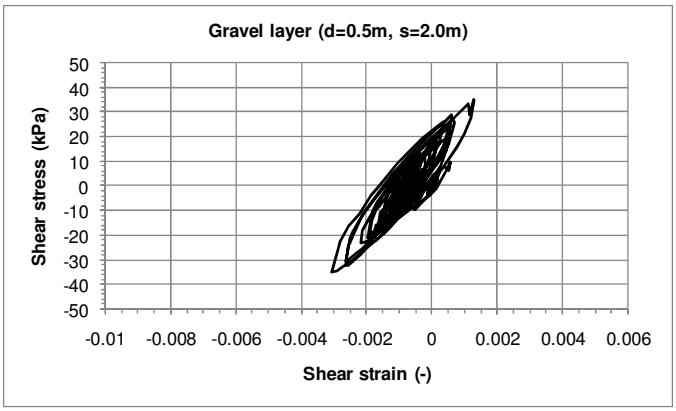

Fig. 22. Shear stress vs. shear strain in gravel layer for DSF (s=2.0 m, d=0.5 m).

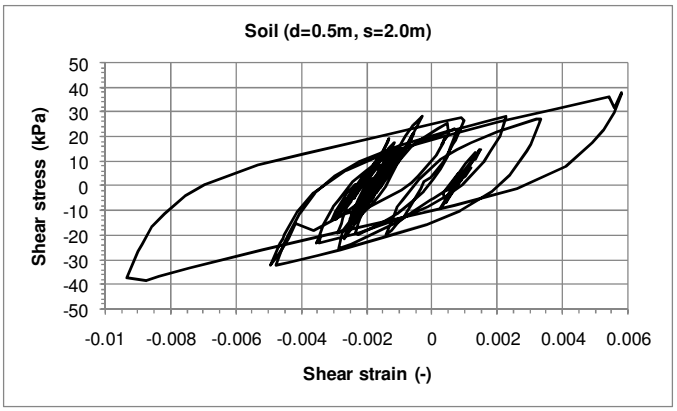

Fig. 24. Shear stress vs. shear strain in soft soil layer underneath gravel (depth=1.0 m) for DSF (s=2.0 m, d=0.5 m).

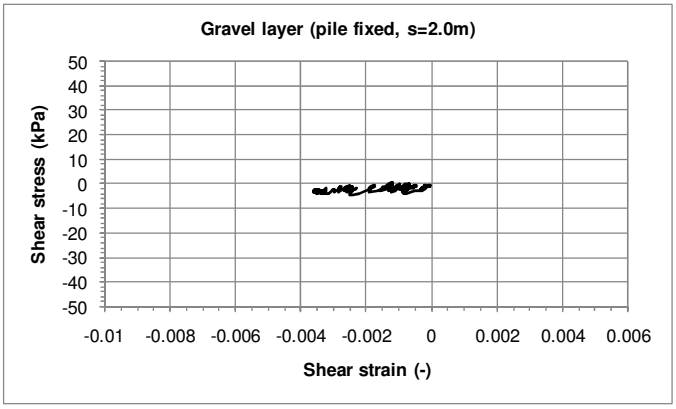

Fig. 23. Shear stress vs. shear strain in gravel layer for fixed connection pile – footing (s=2.0 m).

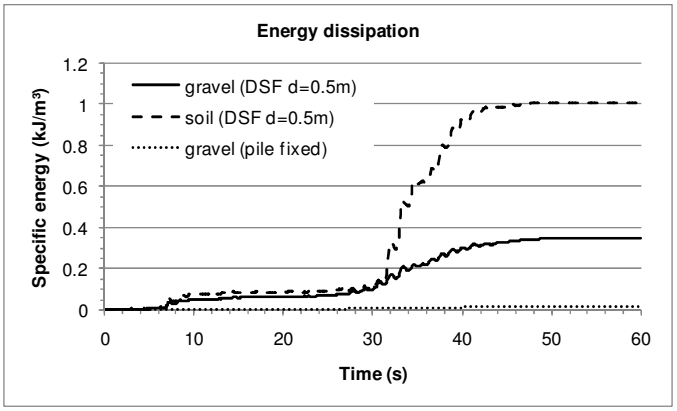

Fig. 25. Specific energy dissipated during earthquake in gravel and soil in case of DSF and pile fixed to footing.

The dissipated energy in the gravel and the soil during the earthquake has been further analyzed and is presented in Fig. 25. The dissipated specific energy E_{diss} (energy per unit volume) due to shearing was roughly estimated as the integral over all shear loops, i.e.

$$E_{diss} = \int_{t_0}^{t_f} \tau(t)\,\dot{\gamma}(t)\,dt \qquad (1)$$

where $\tau(t)$=shear stress, $\dot{\gamma}(t)$=shear strain rate, t_0=time at begin of seismic excitation, t_f=time at end of seismic excitation.

As can be seen in Fig. 25, the DSF allows higher energy dissipation in the gravel compared to the case of the pile fixed to the footing. Nevertheless, the time-displacement response of the point mass and the footing are similar for the DSF and the conventional pile foundation (Fig. 13). Hence, the higher damping of the gravel layer in the DSF does not appear to affect the motion of the footing and superstructure. This can be better understood by comparing the energy dissipated in the gravel and the soft soil. As shown in Fig. 25, E_{diss} of the soft soil exceeds the values of the gravel by a factor of about 3.

Considering that E_{diss} is the specific energy per unit volume, the total energy dissipated in the sheared soft soil mass exceeds the one dissipated in the gravel significantly. Thus, damping perceived by the footing and superstructure is mainly controlled by the hysteretic damping of the soft soil. The contribution of the gravel layer is negligible.

FINAL REMARKS

The behavior of a DSF subjected to a strong earthquake was investigated. The study was focused on the identification of the governing mechanisms and the quantification of the influence of pile spacing and gravel layer thickness on the dynamic response of the DSF.

From the soil mechanics point of view, the seismic response of a DSF is governed by two main mechanisms:

1. Sliding at the footing-gravel layer interface
2. Alternating shearing with decay of shear stiffness in the gravel layer

In a different way, the activation of these mechanisms results in (hysteretic) damping and a decoupling of improved ground

and foundation motion and, therefore a limitation of seismic shear force transmission to the superstructure.
Sliding occurs when the shear force at the interface reaches the sliding resistance, which is governed by the interface friction and the normal force at the contact. During sliding the shear force remains nearly unchanged and the motion of the foundation and ground decouples. A "plastic shear hinge" develops at the interface. Since the direction of motion may reverse many times during the earthquake, sliding does not necessarily lead to failure as in the case of a foundation subjected to horizontal static loads, but it may cause permanent displacements of the foundation. Nevertheless, since a DSF will be generally designed to resist sliding, decoupling of motion due to sliding is actually not expected to occur.

During strong seismic events alternating shearing of the gravel causes a decay of shear stiffness that hinders the passage of shear waves through the gravel layer. If the magnitude of shear strain is large enough this mechanism also leads to decoupling of ground and foundation motion. In this case, the gravel layer acts as an isolator. Prerequisite is that the shear stiffness of the gravel becomes smaller than that of the improved soft ground. The isolation could be improved, if pore pressure develops in the granular layer during the earthquake, since in this case the decay of shear stiffness induced by seismic shaking is stronger.

In our simulations a decoupling of ground and foundation motions did not take place, independent of pile spacing and gravel layer thickness, as none of the two mentioned mechanisms could actually be activated during the earthquake:

1. only small sliding was required to mobilize substantial shear forces at the interface footing-gravel, i.e. the sliding resistance was not reached during the earthquake,
2. in spite of some degradation, the shear stiffness in the gravel layer was much larger than that of the soft soil-piles composite.

We conclude that in general, the mere presence of a gravel layer in a DSF does neither guarantee a decoupling of ground and foundation nor a reduction of inertial forces on the superstructure with respect to the case in which the foundation is fixedly connected or rests directly on the piles. Decoupling in a very soft soil can only occur if the piles significantly contribute to the shear stiffness of the improved soil (very small pile spacing).

The separation of footing and piles by a gravel layer leads to a drastic decrease of bending moments and shear forces induced in the piles during the earthquake. Both the bending moments and the shear forces increase with decreasing pile spacing. During foundation design the pile spacing will have to be optimized based on requirements with respect to vertical bearing behavior as well as moment and shear force loading due to horizontal earthquake loading. The thickness of the gravel layer was not found to influence significantly the bending moment and shear force induced in the piles. This is attributed to the relatively high shear stiffness in the gravel layer in comparison with the improved soft soil below it.

In our numerical analysis the gravel layer was modeled as perfectly drained material (no development of excess pore pressure). In the case of greater foundation dimensions and complete saturation, this assumption might not be justifiable (e.g. Rion-Antirion-Bridge foundation diameter=90 m). Particularly underneath the center of a large footing the drainage path is comparatively long. During strong shaking this could lead to a significant decay of shear stiffness due to the development of excess pore pressure. In the case that saturation of the separation layer can be constantly guaranteed, a possible optimization of the DSF would be to use finer granular material (e.g. a well graded mixture of gravel, sand and silt) instead of gravel to allow a build-up of excess pore water pressure during the earthquake. This isolation principle is similar to the *hanchiku*, a seismic isolation applied in medieval Japan (Pralle, 2002).

ACKNOWLEDGEMENTS

The numerical investigation of the DSF was carried in the framework of an internal research and development project of Bilfinger Berger Civil. The finite element calculations were carried out with the program ABAQUS v6.8. The applied user subroutine containing the visco-hypoplastic and hypoplastic constitutive models was implemented by Dr. A. Niemunis, University of Karlsruhe, Germany.

REFERENCES

Bühler, M. M. [2006]. *"Experimental and Numerical Investigation of the Soil-Foundation-Structure Interaction during Monotonic, Alternating and Dynamic Loading"*. PhD thesis, Institute für Soil Mechanics and Rock Mechanics, University of Karlsruhe, No. 165.

Cudmani, R., V. Osinov, M. M. Bühler, G. Gudehus [2003]. *„A model for evaluation of liquefaction susceptibility in layered soils due to earthquakes"*. Proceedings of the 12th Panamerican Conference on SMGE, Cambridge/USA, Vol. 2, pp. 969-976.

Gudehus, G., R. Cudmani, A. B. Libreros-Bertini, M. M. Bühler, [2004]. *"In-plane and anti-plane strong shaking of soil systems and structures"*. Soil Dynamics and Earthquake Engineering, Vol. 24, pp. 319-342.

Herle, I. and G. Gudehus [1999]. *"Determination of parameters of a hypoplastic constitutive model from properties of grain assemblies"*. Mechanics of Cohesive-Frictional Materials, Vol. 4, No. 5, pp. 461-486.

Karcher, C. [2003]. *„Tagebaubedingte Deformationen im Lockergestein“*. PhD thesis, Institute für Soil Mechanics and Rock Mechanics, University of Karlsruhe, Germany, No. 160.

Libreros Bertini, A. B. [2006]. *“Hypo- und viskohypo-plastische Modellierung von Kriech- und Rutschbewegungen, besonders infolge Starkbeben”*. PhD thesis, Institute für Soil Mechanics and Rock Mechanics, University of Karlsruhe, Germany, No. 166.

Lunne, T., P. K. Robertson and J. J. M. Powell [1997]. “*Cone Penetration Testing in Geotechnical Practice*”. Blackie Academic and Professionals, London.

Mayne, P. W. [1991]. “*Determination of OCR in clays by piezocone tests using cavity expansion and critical state concepts”*. Soils and Foundations, Vol. 31, No. 2, pp. 65-76.

Niemunis, A. and I. Herle [1997]. *“Hypoplastic model for cohesionless soils with elastic strain range”*. Mechanics of Cohesive-Frictional Materials, Vol. 2, No. 4, pp. 279-299.

Niemunis, A. [2003]. *“Extended hypoplastic models for soils“*. Institut für Grundbau und Bodenmechanik der Ruhr-Universität Bochum, Germany, No. 34.

Pecker, A. [2004]. „*Design and construction oft he Rion Antirion Bridge“, Proc. ASCE Geo-Trans 2004,* Los Angeles, CA, USA.

Pralle, N. [2002]. “*Mechanisms in nearly saturated sandy soils under quasi-static dynamic loading”*. PhD thesis, Institute for Soil Mechanics and Rock Mechanics, University of Karlsruhe, Germany, No. 158.

Schünemann, A. [2006]. “*Numerische Modelle zur Beschreibung des Langzeitverhaltens von Eisenbahnschotter unter alternierender Beanspruchung*“. PhD thesis, Institute for Soil Mechanics and Rock Mechanics, University of Karlsruhe, Germany, No. 168.

Vucetic, M. and R. Dobry [1991]. “*Effect of Soil Plasticity on Cyclic Response*”. Journal of Geotechnical Engineering ASCE, Vol. 117, No. 1, pp. 89-107.